Applied Surface Science 310 (2014) 158–163

Contents lists available at ScienceDirect

Applied Surface Science

journal homepage: www.elsevier.com/locate/apsusc

Surface modification by metal ion implantation forming metallic nanoparticles in an insulating matrix

M.C. Salvadori [a,*], F.S. Teixeira [a], L.G. Sgubin [a], M. Cattani [a], I.G. Brown [b]

[a] Institute of Physics, University of Sao Paulo, C.P. 66318, CEP 05314-970, Sao Paulo, S.P., Brazil
[b] Lawrence Berkeley National Laboratory, Berkeley, CA 94720, USA

ARTICLE INFO

Article history:
Received 28 November 2013
Received in revised form 24 March 2014
Accepted 24 March 2014
Available online 31 March 2014

Keywords:
Surface modification
Nanocomposites
Nanoparticles
Ion implantation

ABSTRACT

There is special interest in the incorporation of metallic nanoparticles in a surrounding dielectric matrix for obtaining composites with desirable characteristics such as for surface plasmon resonance, which can be used in photonics and sensing, and controlled surface electrical conductivity. We have investigated nanocomposites produced by metal ion implantation into insulating substrates, where the implanted metal self-assembles into nanoparticles. The nanoparticles nucleate near the maximum of the implantation depth profile (projected range), which can be estimated by computer simulation using the TRIDYN code. TRIDYN is a Monte Carlo simulation program based on the TRIM (Transport and Range of Ions in Matter) code that takes into account compositional changes in the substrate due to two factors: previously implanted dopant atoms, and sputtering of the substrate surface. Our study show that the nanoparticles form a bidimentional array buried a few nanometers below the substrate surface. We have studied Au/PMMA (polymethylmethacrylate), Pt/PMMA, Ti/alumina and Au/alumina systems. Transmission electron microscopy of the implanted samples show that metallic nanoparticles form in the insulating matrix. These nanocomposites have been characterized by measuring the resistivity of the composite layer as a function of the implantation dose. The experimental results are compared with a model based on percolation theory, in which electron transport through the composite is explained by conduction through a random resistor network formed by the metallic nanoparticles. Excellent agreement is found between the experimental results and the predictions of the theory. We conclude in that the conductivity process is due only to percolation (when the conducting elements are in geometric contact) and that the contribution from tunneling conduction is negligible.

Introduction

Nanocomposites formed by metal nanoparticles embedded in an insulating matrix possess interesting electrical, optical, and chemical properties and have potential applications in areas such as electronics, photonics, and biosensing [1–6]. According to a number of theories of transport in isotropic percolating materials [7], the electrical conductivity σ of a composite, near the critical conductor–insulator transition, is given by the scaling law.

$$\sigma \approx \sigma_0(x - x_c)^t \quad (1)$$

where σ_0 is the saturation conductivity for which the material still remains a composite, x is the normalized metal atom concentration of the conducting phase, x_c is the normalized critical concentration, or percolation threshold, below which the composite has the same conductivity as the insulating host material, and t is the critical exponent. For nanocomposite materials formed by metal ion implantation into an insulator, the normalized metal atom concentration x is given by the ion implantation dose ratio φ/φ_0, where φ is the implantation dose and φ_0 (the saturation dose) is the maximum dose for which the material still remains a composite; for doses greater than φ_0 ($x = \varphi/\varphi_0 > 1$), a metal film starts to be deposited on the insulator surface and the material begins to take on the characteristics of a thin metal film.

Electron transport through granular materials consisting of small conducting regions embedded in an insulating medium can occur through either of two possible processes or their combination. When the conducting elements are in geometric contact, theory predicts that the critical exponent t is less than 2 and the process is called percolation [7]; percolation refers to the flow of current through random resistor networks. When the conducting elements are not in geometric contact, inter-particle tunneling

* Corresponding author. Tel.: +55 11 3091 6857; fax: +55 11 3091 6749/+55 11 9964 98841.
E-mail addresses: mcsalvadori@if.usp.br, mcsalvadori08@gmail.com (M.C. Salvadori).

http://dx.doi.org/10.1016/j.apsusc.2014.03.145
0169-4332/

is dominant. Both processes may contribute separate percolation and tunneling currents; then the theory predicts that the critical exponent t is greater than 2 and the process is called tunneling-percolation. Importantly, note that in these critical percolation phenomena we distinguish three regimes: (1) conductor ($x > x_c$), (2) transition ($x \approx x_c$), and (3) insulator ($x < x_c$). In the conducting regime the composite behaves like a dirty metal; the resistivity is relatively low and the temperature coefficient of the resistivity is positive. A vast class of disordered conducting-insulating materials has been analyzed in the last thirty years. It has been shown [7] that the critical parameters t and x_c vary in the ranges $1.5 \leq t \leq 11$ and $0.05 \leq x_c \leq 0.5$. These various composites include carbon-black-polymer systems, oxide-based thick film resistors, and other metal-inorganic and metal-organic insulator composites.

Here we report our investigations of nanocomposites produced by metal ion implantation into insulating substrates, where the implanted metal self-assembles into nanoparticles. Stepanov and coworkers [8] have described the formation of silver nanoparticles in glass by ion implantation near room temperature; their paper contains a detailed analysis and description of the nanoparticle formation process. An excess of neutral metal atoms above the solubility limit leads to nucleation and growth of metal particles, driven by the temperature and temperature gradients within the implanted sample including the beam-induced thermal characteristics. The nanoparticles nucleate near the maximum of the implantation depth profile (projected range).

The implantation depth profile can be estimated by computer simulation using the TRIDYN code [9,10]. This is a Monte Carlo simulation program based on the TRIM (transport and range of ions in matter) code [11]. TRIDYN takes into account compositional changes in the substrate due to two factors: previously implanted dopant atoms, and sputtering of the substrate surface. The TRIDYN program is appropriate when the substrate composition changes significantly during the implantation process, as occurs for moderate-to-high implantation dose.

Specifically, we have studied the nanocomposite systems Au/PMMA (polymethylmethacrylate) [12–19], Pt/PMMA [20], Ti/alumina [21] and Au/alumina [22]. PMMA is an important polymer as it is widely used as an electron resist for high resolution lithography [23], and PMMA modified with metal nanoparticles widens significantly its application potential. Alumina is used for fabricating high-voltage insulators including, for example, high voltage accelerator columns and support rods for electrostatic focusing lenses in single-ion devices. For these applications, it is very useful to have control over the surface resistivity (sheet resistance) of the material; the goal is to remove charge accumulation from the surface or, said differently, to grade the voltage drop along the surface in a uniform and controlled way. Metal ion implantation into alumina has been used for these purposes and the approach has met with considerable success [24,25]. Our work, reported here, contributes to the theoretical understanding of the physics involved in this empirical approach. Gold and platinum were chosen for ion implantation because of their chemical stability, and titanium was used because of its low cost.

The aim of this paper is to summarize and compare the characteristics of the different nanocomposites obtained by metal ion implantation into insulating materials, highlighting those similar characteristics for nanocomposites formed with the same matrix (insulator).

Nanocomposite systems investigated

Au/PMMA system

The ion implantation targets were fabricated from glass microscope slides that were cut into $15 \times 6\ mm^2$ pieces. PMMA (950 k A2, from Microchem Corp.) was then deposited on the samples using a spin coater. The PMMA film thickness was about 50 nm. Electrical contacts were formed at both ends of the substrates using silver glue followed by plasma deposition of relatively thick (200 nm) platinum films onto the contacts, with a mask protecting the center of the samples, as shown in Fig. 1, where $\ell \sim w \sim 6$ mm.

Fig. 1. Schematic of the implantation targets on which the conducting polymer samples are formed.

Very low energy (49 eV) was used for ion implantation into PMMA. We used a streaming (unidirectionally drifting) charge–neutral plasma formed by a vacuum arc plasma gun. It is a characteristic of vacuum arc plasmas that the metal plasma, formed at the cathode of the discharge, has a directed ion energy typically in the range 20–200 eV, depending on the cathode material and thus the metal plasma ion species; for Au the ion drift energy is 49 eV [26,27]. The vacuum arc plasma technique used by us has been fully described elsewhere [28,29]. Briefly, a repetitively-pulsed vacuum arc plasma gun equipped with a gold cathode was used to form a dense gold plasma which was then transported through a 90° bent-solenoidal magnetic filter to remove any solid particulates (cathode debris) from the plasma stream. The substrate was positioned near the exit of the filter. For the work described here the plasma pulses were 5 ms long and the repetition rate was 1 pulse/s. For Au ion implantation at 49 eV into PMMA, the buried layer is only about 6 nm deep (below the surface of the PMMA) and of width (FWHM) about 3 nm, as determined by the TRIDYN code. The implanted ion dose φ was determined from the number of plasma pulses, using a prior calibration involving measurement of deposited film thickness as a function of number of pulses.

Three similar experiments were carried out. The sample resistances were measured throughout the gold ion implantation process, thus determining the sample conductivity as a function of ion implantation dose.

Typical results from our experiments are shown in Fig. 2, where the measured conductivity ratio σ/σ_0 is plotted as a function of the normalized concentration x. For all samples the maximum dose φ_0 was found to be $\varphi_0 = 2 \times 10^{16}\ cm^{-2}$; at this dose the composite conductivity assumes its maximum value σ_0. Data such as that of Fig. 2 were obtained for the three separate samples. These curves of σ/σ_0 as a function of x are similar to those observed by other

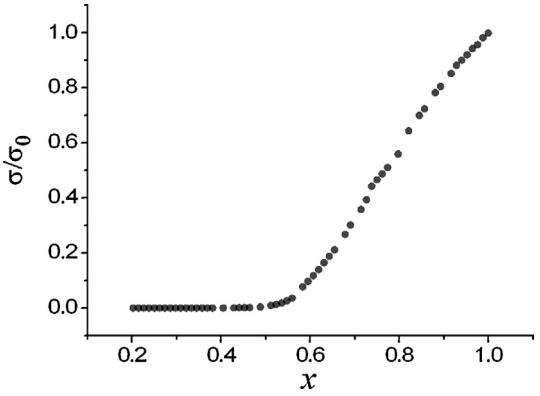

Fig. 2. Measured conductivity ratio σ/σ_0 as a function of normalized gold atom concentration x for one of the Au/PMMA samples.

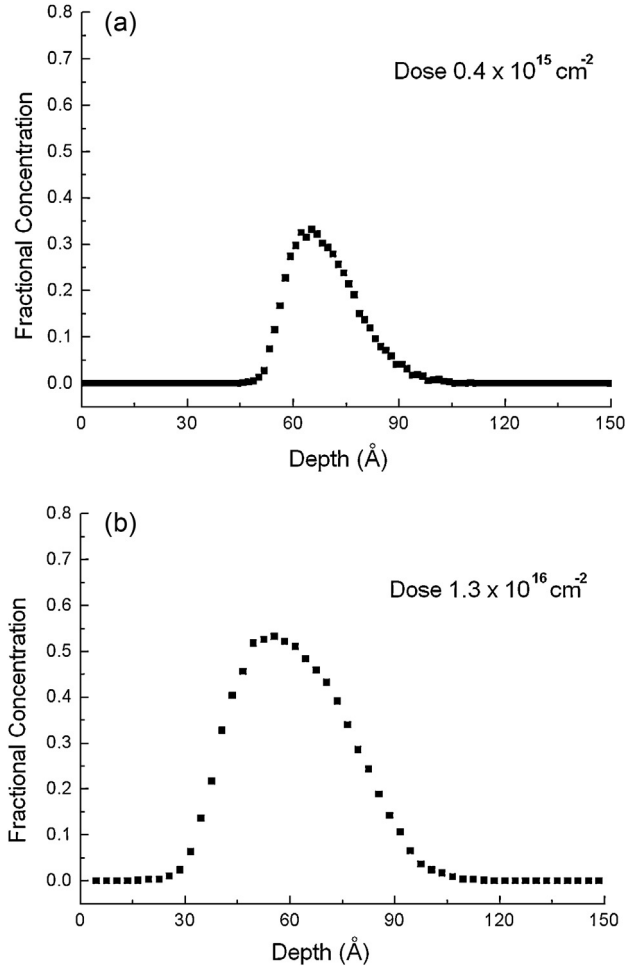

Fig. 3. TRIDYN simulations for samples with gold doses of (a) 4.4×10^{15} and (b) 1.3×10^{16} ions/cm^2 showing the depth profiles.

workers for metal/insulator composites in the percolation regime [7].

The percolation threshold x_c obtained from Fig. 2 is 0.49. At this critical point the implanted gold ion dose (or percolation dose φ_c) is about 1×10^{16} atoms/cm^2. The data of Fig. 2 and the threshold $x_c = 0.49$ were used to determine the parameter t, fitting Eq. (1). The value obtained was $t = 1.64$. The same procedure was used for the two other samples. Taking into account the results obtained for all three samples, the critical concentration was $x_c = 0.45 \pm 0.05$ and the critical exponent was $t = 1.66 \pm 0.02$.

Our measured x_c and t values are in good agreement with experimental values found in the literature for metal ions implanted into polymers or insulators [7] and also with predicted t values for a simple cubic lattice that have been given as $t = 1.5 \pm 0.2$, $t = 1.6 \pm 0.1$ and $t = 1.69 \pm 0.03$ by Kirkpatrick [30,31], Sur et al. [32] and Levinshtein et al. [33], respectively. Since the critical exponent obeys the condition $t < 2.0$, we conclude [7] that in our PMMA samples implanted with low energy gold ions the conductivity process is due only to percolation and that the contribution from tunneling conduction is negligible.

The TRIDYN-calculated depth profiles for two different doses (4.4×10^{15} and 1.3×10^{16} ions/cm^2) are shown in Fig. 3. It can be seen that the simulation with higher dose shows a greater buried gold layer width and magnitude (fractional gold content within the buried layer). Other TRIDYN simulations that we have explored show that a gold surface film begins to form for dose greater than about 1×10^{17} cm^{-2}.

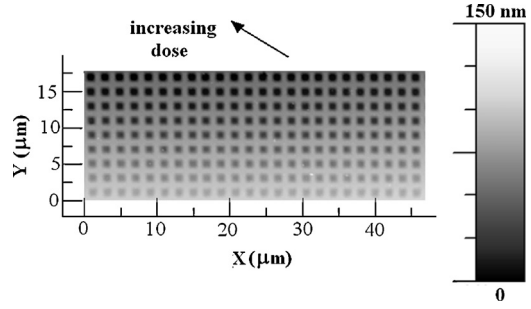

Fig. 4. AFM image of the contrast pattern produced on PMMA after gold implantation at a dose of 1.3×10^{16} atoms/cm^2. Electron beam dose was from 10 to 46 μC/cm^2.

Electron beam lithography was performed on the Au/PMMA system [18] using a scanning electron microscope (Jeol Model JSM-6460 LV) controlled by a Nanometer Pattern Generation System (NPGS). As a suitable pattern for contrast studies, a standard grid pattern with periodicity of 2 μm was used. For each 1 μm^2 square of the grid a different electron dose was used. The electron beam current was 10 pA, corresponding to a Gaussian beam of diameter about 70 nm. The electron dose was varied from 10 μC/cm^2 to 46 μC/cm^2 in 4 μC/cm^2 steps, thus providing a 2-D pattern allowing us to obtain the lithographic contrast properties. The patterns obtained for each sample were visualized by AFM. A typical image is shown in Fig. 4. In these images, each pad (1 μm × 1 μm square) corresponds to a PMMA region modified by the electron beam and developed. The step height visible in the image corresponds to the lithographic electron beam dose used. This approach allows us to identify the minimum electron dose that can be used for completely removing the PMMA within each affected area, so yielding the best spatial resolution for the desired pattern. Twelve samples of PMMA films were prepared on silicon substrates and gold ion implantation was performed over a range of 4.4×10^{15} up to 3.6×10^{16} atoms/cm^2.

The electron beam lithography contrast curves obtained were essentially the same for all 12 implanted samples, as well as for one unimplanted sample. In Fig. 5 we show the average contrast curve—normalized resist thickness as a function of the logarithm of electron exposure dose. The normalized resist thickness is the polymer thickness remaining after electron beam exposure divided by the original polymer thickness, both measured by AFM. These results indicate that the gold-implanted PMMA samples, for ion doses between 4.4×10^{15} cm^{-2} and 3.6×10^{16} cm^{-2}, all have

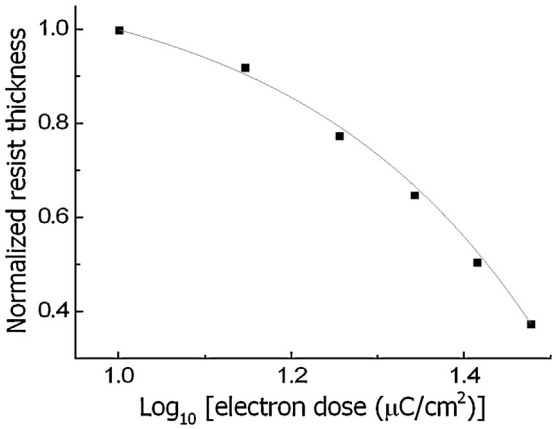

Fig. 5. Lithographic contrast curve—normalized resist thickness (polymer thickness remaining after electron beam exposure, divided by the original polymer thickness) as a function of the logarithm of electron exposure dose. The curve plotted is the average over all implantation doses investigated here.

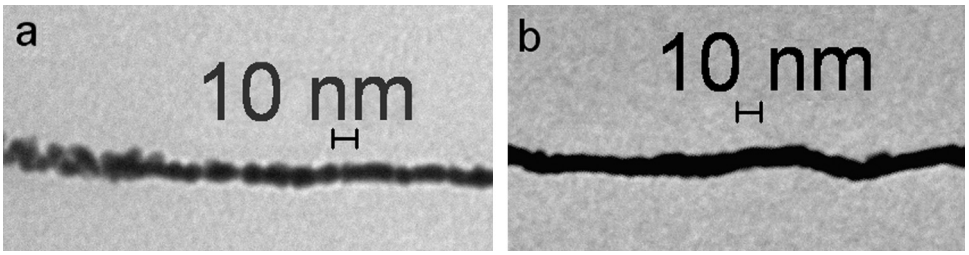

Fig. 6. TEM cross-section images of buried layer profiles for samples of Au/PMMA with implantation doses: (a) 0.8×10^{16} atoms/cm^2 and (b) 1.5×10^{16} atoms/cm^2.

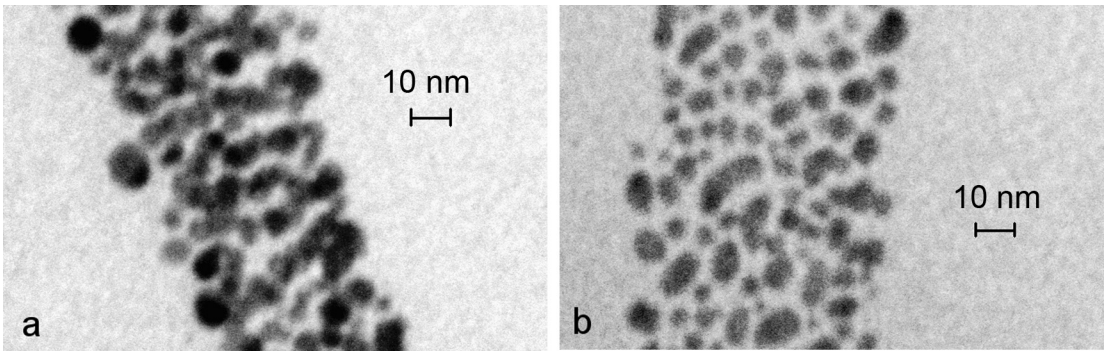

Fig. 7. Top-view TEM images for samples of Au/ PMMA with implantation doses: (a) 0.8×10^{16} atoms/cm^2 and (b) 1.5×10^{16} atoms/cm^2.

Table 1
Summary of TRIDYN predictions and TEM measurements for samples of Au/PMMA composites with Au doses of 0.8×10^{16} atoms/cm^2 and 1.5×10^{16} atoms/cm^2.

Au/PMMA nanocomposite		Sample with Au dose $\phi = 0.80 \times 10^{16}$ atoms/cm^2 (nm)	Sample with Au dose $\phi_2 = 1.5 \times 10^{16}$ atoms/cm^2 (nm)
Simulated	TRIDYN buried layer width (L)	6.0	7.5
Experimental	TEM buried layer width (L)	5.5	7.8
	Mean cluster diameter (D_{mean})	5.1	6.3

similar lithographic properties. Thus the modified PMMA formed in our experiments is a suitable bi-layer material that can be e-beam lithographed to generate uniform surfaces; the buried gold layer does not lead to any property changes with respect to e-beam lithography.

Transmission electron microscopy (TEM) of the Au/PMMA system showed that the buried layer width was between about 6 and 8 nm and the cluster diameter was between about 5 and 6 nm for doses between 0.8×10^{16} atoms/cm^2 and 1.5×10^{16} atoms/cm^2, as illustrated in Figs. 6 and 7.

Table 1 summarizes the TRIDYN simulation predictions for the buried layer width and the TEM measurements for samples of Au/ PMMA composites with Au doses of 0.8×10^{16} atoms/cm^2 and 1.5×10^{16} atoms/cm^2. Note that the predicted layer widths are in good agreement with the widths measured from the TEM images. As the mean cluster diameter is just a little less than the buried layer thickness, we can conclude that the nanocomposite layer of Au/PMMA is basically a two dimensional array of nanoparticles below the PMMA surface.

Pt/PMMA system

A similar approach was used for studying the Pt/PMMA nanocomposite. Fig. 8 shows the measured conductivity ratio σ/σ_0 as a function of normalized Pt atom concentration x for one of the Pt/PMMA samples. The Pt implantation energy into PMMA was 67 eV and the saturation dose obtained was $\varphi_0 = 1.6 \times 10^{16}$ atoms/cm^2, the percolation dose was $\varphi_c = 0.5 \times 10^{16}$ atoms/cm^2, generating $x_c = \varphi_c/\varphi_0 = 0.31$, and the critical exponent obtained was $t = 1.46$. Similarly to the nanocomposite Au/PMMA $t < 2.0$ suggesting that the conductivity is due only to percolation.

Fig. 9 shows a top-view TEM image for a sample of Pt/PMMA nanocomposite with Pt dose 0.4×10^{16} atoms/cm^2, showing the presence of nanoparticles with sizes less than 10 nm.

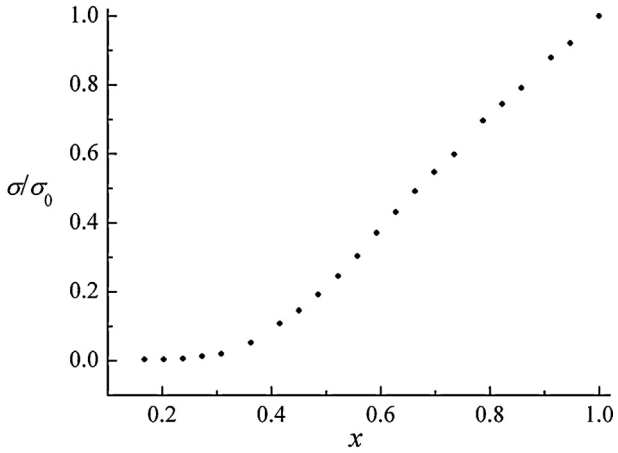

Fig. 8. Measured conductivity ratio σ/σ_0 as a function of normalized Pt atom concentration x for one of the Pt/PMMA samples.

Table 2
Saturation dose, φ_0, saturation conductivity, σ_0, normalized percolation dose x_c, percolation dose, φ_c, and critical exponent t for Au/PMMA, Pt / PMMA, Ti/alumina and Au/alumina composites. The ion implantation energy was 49 eV for Au into PMMA, 67 eV for Pt into PMMA, 75 keV for Ti into alumina and 40 keV for Au into alumina.
* Estimated value

Composite	φ_0 (cm^{-2})	σ_0 (S/m)	$x_c = \varphi_c/\varphi_0$	φ_c (cm^{-2})	t
Au/PMMA	2×10^{16}	2.0×10^{6}	0.50	1×10^{16}	1.64
Pt/PMMA	1.6×10^{16}	0.5×10^{6}	0.31	0.5×10^{16}	1.46
Ti/alumina	10×10^{16}	50	0.4*	4×10^{16}	–
Au/alumina	9.5×10^{16}	14	0.46	4.4×10^{16}	1.4

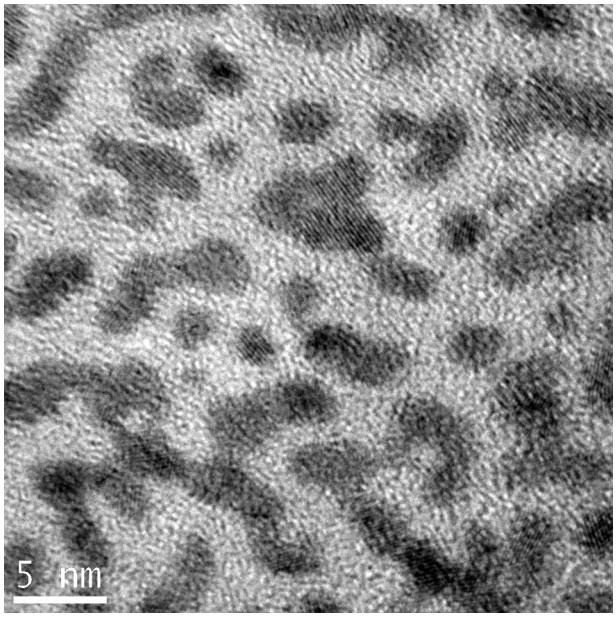

Fig. 9. Top-view TEM image for a sample of Pt/PMMA nanocomposite with Pt dose 0.4×10^{16} atoms/cm^2.

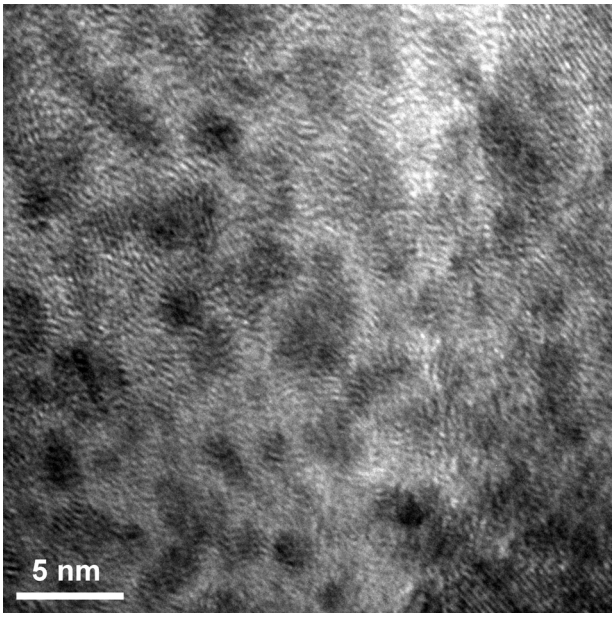

Fig. 10. Top-view TEM image for a sample of Au / alumina nanocomposite with Au dose of 4.8×10^{16} atoms/cm^2.

Au/alumina system

The Au/alumina system was formed by implanting Au into alumina at a higher energy of 40 keV. The measured conductivity ratio σ/σ_0 as a function of normalized Au atom concentration x for two Au/alumina samples was very similar to that derived from the curves obtained for Au/PMMA and Pt/PMMA. The saturation dose obtained was $\varphi_0 = 9.5 \times 10^{16}$ atoms/cm^2, the percolation dose was $\varphi_c = 4.4 \times 10^{16}$ atoms/cm^2, generating $x_c = \varphi_c/\varphi_0 = 0.46$, and the critical exponent obtained was $t = 1.4$. In this case $t < 2.0$, suggesting once again that the conductivity is due only to percolation.

Fig. 10 shows a top-view TEM image for a sample of Au/alumina nanocomposite with Au dose 4.8×10^{16} atoms/cm^2, showing the presence of nanoparticles with sizes lower than 10 nm.

Ti/alumina system

The Ti/alumina system was formed by implanting Ti into alumina at an ion energy of 75 keV. In this case just four samples were prepared and, based in our prior results, the percolation parameters were estimated.

Table 2 presents a summary of all results obtained in this work.

One can see from the table that, although having similar values for the normalized percolation dose x_c and the critical exponent t, we have very different values for the saturation dose φ_0, percolation dose φ_c and saturation conductivity σ_0 of the composites. The composites with alumina have a saturation dose and percolation dose about 4 up to 9 times greater than for the composites with PMMA. In addition, the saturation conductivities σ_0 of the composites with alumina are about 10^4 up to 10^5 times lower than for the composites with PMMA. With these results we can conclude that the alumina composites have higher resistivity than the PMMA composites, still both being percolated systems.

Conclusion

We have formed Au/PMMA, Pt/PMMA, Au/alumina and Ti/alumina nanocomposites using ion implantation and investigated their characteristics. All the systems contain nanoparticles smaller than 10 nm, generating metal/insulator nanocomposites. The percolation parameters were determined and the electrical properties of the nanocomposites measured.

Acknowledgments

This work was supported by Fundação de Amparo a Pesquisa do Estado de São Paulo (FAPESP) and Conselho Nacional de Desenvolvimento Científico e Tecnológico (CNPq).

References

[1] G. Mie, Beiträge zur Optik trüber Medien, speziell kolloidaler Metallösungen, Ann. Phys. 330 (1908) 377–445.
[2] A. Heilmann, Polymer Films with Embedded Metal Nanoparticles, Springer, New York, NY, 2008.
[3] S. Maier, Plasmonics: Fundamentals and Applications, Springer, Berlin, 2007.
[4] U. Kreibig, M. Vollmer, Optical Properties of Metal Clusters, Springer, Berlin, 1995.
[5] L. Nicolais, G. Carotenuto, Metal-Polymer Nanocomposites, Wiley, Hoboken, NJ, 2005.
[6] I.H. El-Sayed, X. Huang, M.A. El-Sayed, Surface plasmon resonance scattering and absorption of anti-EGFR antibody conjugated gold nanoparticles in cancer diagnostics: applications in oral cancer, Nano Lett. 5 (2005) 829–834.

[7] S. Vionnet-Menot, C. Grimaldi, T. Maeder, S. Strässler, P. Ryser, Tunneling-percolation origin of nonuniversality: theory and experiments, Phys. Rev. B: Condens. Matter 71 (2005) 064201.
[8] A.L. Stepanov, D.E. Hole, P.D. Townsend, Formation of silver nanoparticles in soda-lime silicate glass by ion implantation near room temperature, J. Non-Cryst. Solids 260 (1999) 65–74.
[9] W. Möller, W. Eckstein, Tridyn—a TRIM simulation code including dynamic composition changes, Nucl. Instrum. Methods Phys. Res. B 2 (1984) 814–818.
[10] W. Möller, W. Eckstein, J.P. Biersack, Tridyn-binary collision simulation of atomic collisions and dynamic composition changes in solids, Comput. Phys. Commun. 51 (1988) 355–368.
[11] J.F. Ziegler, J.P. Biersack, U. Littmark, The Stopping and Range of Ions in Solids, Pergamon Press, New York, NY, 1985 (new edition in 1996). The computer code is downloadable from the SRIM website http://www.srim.org/.
[12] F.S. Teixeira, M.C. Salvadori, M. Cattani, I.G. Brown, Annealing effects on nanostructured gold–polymethylmethacrylate composites: small-angle x-ray scattering analysis, J. Appl. Phys. 111 (2012) 104311.
[13] J. Ferreira, F.S. Teixeira, A.R. Zanatta, M.C. Salvadori, R. Gordon, O.N. Oliveira Jr., Tailored SERS substrates obtained with cathodic arc plasma ion implantation of gold nanoparticles into a polymer matrix, Phys. Chem. Chem. Phys. 14 (2012) 2050–2055.
[14] F.S. Teixeira, M.C. Salvadori, M. Cattani, I.G. Brown, Structure of disordered gold-polymer thin films using small angle x-ray scattering, J. Appl. Phys. 108 (2010) 093505.
[15] F.S. Teixeira, M.C. Salvadori, M. Cattani, I.G. Brown, Electrical, optical and structural studies of shallow buried Au–PMMA composite films formed by very low energy ion implantation, J. Vac. Sci. Technol., A 28 (2010) 818–823.
[16] F.S. Teixeira, M.C. Salvadori, M. Cattani, S.M. Carneiro, I.G. Brown, Surface plasmon resonance of gold nanoparticles formed by cathodic arc plasma ion implantation into polymer, J. Vac. Sci. Technol., B 27 (2009) 2242–2247.
[17] F.S. Teixeira, M.C. Salvadori, M. Cattani, I.G. Brown, Structural properties of buried conducting layers formed by very low energy ion implantation of gold into polymer, J. Appl. Phys. 106 (2009) 056106.
[18] F.S. Teixeira, M.C. Salvadori, M. Cattani, I.G. Brown, Gold-implanted shallow conducting layers in PMMA, J. Appl. Phys. 105 (2009) 064313.
[19] M.C. Salvadori, M. Cattani, F.S. Teixeira, I.G. Brown, Conducting polymer formed by low energy gold ion implantation, Appl. Phys. Lett. 93 (2008) 073102.
[20] M.C. Salvadori, F.S. Teixeira, M. Cattani, I.G. Brown, Electrical conductivity of platinum-implanted polymethylmethacrylate nanocomposite, J. Appl. Phys. 110 (2011) 114905.
[21] M.C. Salvadori, F.S. Teixeira, M. Cattani, A. Nikolaev, K.P. Savkin, E.M. Oks, H.-K. Park, L. Phillips, K.M. Yu, I.G. Brown, On the electrical conductivity of Ti-implanted alumina, J. Appl. Phys. 111 (2012) 063714.
[22] M.C. Salvadori, F.S. Teixeira, L.G. Sgubin, M. Cattani, I.G. Brown, Electrical conductivity of gold-implanted alumina nanocomposite, Nucl. Instrum. Methods Phys. Res. Sect. B 310 (2013) 32–36.
[23] M.J. Madou, Fundamentals of Microfabrication—The Science of Miniaturization, second ed., CRC Press, New York, NY, 2002.
[24] D. Li, J. Zhang, M. Yu, J. Kang, W. Li, Change of sheet resistance of high purity alumina ceramics implanted by Cu and Ti ions, Appl. Surf. Sci. 252 (2005) 1029–1034.
[25] A. Nikolaev, E.M. Oks, K. Savkin, G.Yu. Yushkov, D.J. Brenner, G. Johnson, G. Randers-Pehrson, I.G. Brown, R.A. MacGill, Surface resistivity tailoring of ceramic insulators for an ion microprobe application, Surf. Coat. Technol. 201 (2007) 8120–8122.
[26] D.R. Martins, M.C. Salvadori, P. Verdonk, I.G. Brown, Contamination due to memory effects in filtered vacuum arc plasma deposition systems, Appl. Phys. Lett. 81 (2002) 1969–1971.
[27] A. Anders, G.Y. Yushkov, Ion flux from vacuum arc cathode spots in the absence and presence of a magnetic field, J. Appl. Phys. 91 (2002) 4824–4832.
[28] M.C. Salvadori, I.G. Brown, A.R. Vaz, L.L. Melo, M. Cattani, Measurement of the elastic modulus of nanostructured gold and platinum thin films, Phys. Rev. B: Condens. Matter 67 (2003) 153404.
[29] I.G. Brown, Cathodic Arc deposition of films, Annual Review of Materials Science, 28, Annual Reviews, Inc., Palo Alto, CA, 1998.
[30] S. Kirkpatrick, Classical transport in disordered media: scaling and effective-medium theories, Phys. Rev. Lett. 27 (1971) 1722–1725.
[31] S. Kirkpatrick, Percolation and conduction, Rev. Mod. Phys. 45 (1973) 574–588.
[32] A. Sur, J.L. Lebowitz, J. Marro, M.H. Kalos, S. Kirkpatrick, Monte Carlo studies of percolation phenomena for simple cubic lattices, J. Stat. Phys. 15 (1976) 345–355.
[33] M.E. Levinshtein, B.I. Shklovskii, M.S. Shur, A.L. Efros, The relation between the critical exponents of percolation theory, Zh. Eksp. Theor. Fiz. 69 (1975) 386–394.